Medical Engineering and Physics 49 (2017) 71–78

Contents lists available at ScienceDirect

Medical Engineering and Physics

journal homepage: www.elsevier.com/locate/medengphy

Non-linear finite element model to assess the effect of tendon forces on the foot-ankle complex

Enrique Morales-Orcajo[a,b,c,e,*], Thales R. Souza[d], Javier Bayod[a,b,e], Estevam Barbosa de Las Casas[c]

[a] Group of Structural Mechanics and Materials Modeling (GEMM), Aragón Institute of Engineering Research (I3A). University of Zaragoza, Zaragoza, Spain
[b] Biomedical Research Networking Center in Bioengineering, Biomaterials and Nanomedicine (CIBER-BBN), Spain
[c] Group of Biomechanical Engineering UFMG - (MecBio), School of Engineering, Universidade Federal de Minas Gerais, Belo Horizonte, MG, Brazil
[d] Department of Physical Therapy, Graduate Program in Rehabilitation Sciences, Universidade Federal de Minas Gerais, Belo Horizonte, MG, Brazil
[e] Mechanical Engineering Department, School of Engineering and Architecture (EINA), University of Zaragoza, c/María de Luna s/n, Betancourt Building, 50018 Zaragoza, Spain

ARTICLE INFO

Article history:
Received 11 December 2016
Revised 18 June 2017
Accepted 24 July 2017

Keywords:
Finite element method
Foot tendons
Computational simulation
Hyperelastic behavior
Ogden model
Foot biomechanics

ABSTRACT

A three-dimensional foot finite element model with actual geometry and non-linear behavior of tendons is presented. The model is intended for analysis of the lower limb tendon forces effect in the inner foot structure. The geometry of the model was obtained from computational tomographies and magnetic resonance images. Tendon tissue was characterized with the first order Ogden material model based on experimental data from human foot tendons. Kinetic data was employed to set the load conditions. After model validation, a force sensitivity study of the five major foot extrinsic tendons was conducted to evaluate the function of each tendon. A synergic work of the inversion-eversion tendons was predicted. Pulling from a peroneus or tibialis tendon stressed the antagonist tendons while reducing the stress in the agonist. Similar paired action was predicted for the Achilles tendon with the tibialis anterior. This behavior explains the complex control motion performed by the foot. Furthermore, the stress state at the plantar fascia, the talocrural joint cartilage, the plantar soft tissue and the tendons were estimated in the early and late midstance phase of walking. These estimations will help in the understanding of the functional role of the extrinsic muscle-tendon-units in foot pronation-supination.

1. Introduction

Foot finite element (FE) models have been developed during the last three decades improving their features as computational capacity and constitutive models for biological tissues were improving. Mechanical behavior of bone has been well addressed, but foot soft tissues approaches are still evolving [1]. Advances have been achieved in simulating the non-linear behavior of foot plantar soft tissue and refined constitutive models with real geometries of ligaments are currently used in foot modeling. However, muscle and tendon components have not been appropriately addressed yet [2].

Realistic tendon simulation provides refined estimation of the mechanical performance on the foot-ankle complex. Kinematic and dynamic tendon data can be found in the literature [3–5]. However, stress levels of tendons are rarely reported mainly due to the complexity of performing experimental measurements and the difficulty of modeling soft tissue. Fill this gap is relevant from a clinical perspective since stress helps to estimate pain and tissue damage and it is independent of the structural characteristics of the tendon.

In computational foot modeling, tendon representations have been limited to reaction forces in the tendon insertions [6,7] or the use of one-dimensional link elements [8,9]. Recent approaches included the realistic geometry of Achilles tendon (AT), but the remaining tendons that control foot motion were represented by truss elements or neglected [10]. The consideration of the real tendon geometry allows the study of the tendon itself and not only its reaction in the bone structure. This opens new avenues in the analysis of the foot tendon performance. Furthermore, the use of linear material models to assess the non-linear behavior of tendon tissue is other of the current boundaries in foot tendon simulation. Particularly, in FE foot modeling, only three different approaches have been used for this tissue [2]. The first approach was presented by Wu [11] in a 2D foot FE model where the tendon tissue was configured linear elastic transverse isotropic using a Young's modulus

* Corresponding author at: Mechanical Engineering Department, School of Engineering and Architecture (EINA), University of Zaragoza, c/María de Luna s/n, Betancourt Building, 50018 Zaragoza, Spain.
E-mail address: enriquem@unizar.es (E. Morales-Orcajo).

http://dx.doi.org/10.1016/j.medengphy.2017.07.010
1350-4533/

of 1200 MPa for the axial direction and a Poisson's ratio of 0.4. The second approach was given by Gu et al. [12] in a 3D model of the Achilles tendon. They simulated the Achilles tendon behavior using an incompressible hyperelastic two-parameter Mooney–Rivlin formulation. The third approach was the isotropic linear elastic material model with Young's modulus of 450 MPa and Poisson's ratio of 0.3 firstly used by Garcia-Aznar et al. [13]. Linear material models are based on the consideration that stresses and strains are proportional. This approximation disregards the initial elongation of the tendons at lower stress values, the so-called toe region [14,15]. As for non-linear material models, that initial strain is considered, as well as the non-linear transition previous to the linear region, providing more realistic stress estimations.

The purpose of this study was to establish a three-dimensional FE model of the human foot using detailed realistic geometry and non-linear behavior of tendons. The model was used to shed light on the role of each tendon in the mechanical response of the foot. For this, force sensitivity analyses of ankle stabilizer tendons, i.e. peroneus, tibialis, and Achilles tendons, were performed. Furthermore, the mechanical solicitations of the internal foot components were predicted at the beginning and the end of the midstance phase of walking. These estimations will help in the understanding of the functional role of the extrinsic muscle-tendon-units of the foot and in the quantification of its mechanical performance.

2. Methods

2.1. Finite element model

2.1.1. Geometry reconstruction

The right foot of a 49 years old male volunteer, with weight of 70 kg and height of 170 cm, was scanned to obtain the geometry of the FE model. Two different tomographies were utilized to capture the geometry details of all tissues in the foot [16]. First, x-ray 0.6 mm slice distance computed tomographic images were segmented to define bone volumes (cortical and trabecular) and to sketch a primary distribution of the tendons. Then, magnetic resonance images, which provide a better definition of soft tissues, were used to refine the initial segmentation, especially the deeper layers of muscles. MIMICS software (Materialise, Leuven, Belgium) was employed to generate the three-dimensional surfaces (STL files) from the two-dimensional stacked image data. This image processing software, frequently cited in three-dimensional reconstruction from medical images [2], use an adapted marching cubes algorithm to create three-dimensional surfaces based on the masks, i.e. region of interest, selected during the segmentation process. Several anatomy references were additionally consulted to help in the identification and delimitation of each individual tendon geometry [17–19].

Due to the complexity of the internal foot components, mostly the intrinsic muscles and tendons concentrated under the foot arch, the reconstructed geometry was processed to avoid volume intersection and other geometrical disruptions before meshing. The detailed segmentation of the foot-ankle complex consists of 102 independent segments corresponding to 30 cortical bone segments, 18 trabecular bone segments, 22 cartilage segments, 29 tendon and muscle segments, 2 fascia segments and the soft tissue volume surrounding the complex (Fig. 1).

2.1.2. Meshing

ANSYS ICEM CFD (ANSYS Inc., Canonsburg, PA, USA) was chosen because of its efficiency in meshing large and complex models and its extended mesh diagnosis. A trial-error approach was employed to optimize the mesh size of each segment. The conditions to achieve a reasonable mesh size without compromising the calculation time were:

- A minimum mesh size sufficiently small to fit into the tightest segments, particularly in the forefoot where many different minor components are concentrated such as proximal, medial and distal phalanges, toes joint cartilages and the thinnest tendons.
- A maximum mesh size consistent with the minimum to avoid large differences in element size between regions and to ensure that the results were independent of the mesh density.
- The mesh accuracy had to achieve more than 99% of the elements better than 0.2 mesh quality (Jacobians) and check that the poor elements were located away from the region of highest interest, i.e. bone, tendon and fascia structures.
- The number of elements below a million. With our current computational capacity (Intel Core i5 3.2 GHz CPU and 4 GB RAM), meshes higher than one million elements increase disproportionally the computational time.

The equilibrium was found with 806.475 linear tetrahedral elements with element sizes as follows: 1 mm for smallest cartilages between phalanges, 2 mm for phalanges, the thinnest tendons and the rest of the cartilages, 3 mm for metatarsals and the rest of the tendons, 4 mm for intrinsic muscles and AT and 5 mm for the large bones in the hindfoot and the fat tissue. This configuration is similar to the 4 mm element size reported by Isvilanonda et al. [8] but optimized for geometry requirements. The quality of the mesh was checked taking as reference the recommendations of Burkhart et al. [20]. All parameters were within good mesh quality ratios (Table 1).

2.1.3. Boundary conditions

The pre-processing of the mesh previous to calculus was conducted with the software I-DEAS (SDRC, Milford, CT, USA). A rigid plane under the foot was included in the model in order to calculate ground reaction forces. A node-to-surface contact between the model and the rigid plane was defined with a friction coefficient of 0.6 [6]. Loads, boundary conditions, calculus, and post-processing were processed using ABAQUS (ABAQUS Inc., Pawtucket, RI, USA). The loads and boundary conditions varied for each analysis and are described in Section 2.4.

2.2. Material properties: tendon characterization

All the material properties used in the model were taken from the literature except for tendon tissue. The constitutive model, the material parameters, and the references are detailed in Table 2. The material model for tendons was determined based on experimental data collected from 100 uniaxial tensile tests of different human foot tendons [15].

Several hyperelastic formulations predefined in ABAQUS were chosen to simulate the actual behavior of human foot tendons. Constitutive models with a smaller number of material parameters were preferred because less experimental tests are required to determine their parameters. Ogden first and second order, Polynomial $n = 1$ and 2, and Polynomial reduced order 1, 2 and 3 formulations were included in the analysis. The material models that fitted the average experimental curve and also performed a real physiological behavior (compression stress with negative strains) were then used to simulate uniaxial tendon tests. The model that showed better agreement with experimental data was chosen.

Once the parameters of the material model for foot tendon tissue were defined, the model performance was compared with previous foot tendon material models reported in the literature: the linear models used by Wu [11] and Garcia-Aznar et al. [13] and the hyperelastic model used by Gu et al. [12]. Four simple one-dimensional models were created with the structural properties of four randomly selected tendon samples from a previous experimental study [15] to replicate the tests. Each model was run four

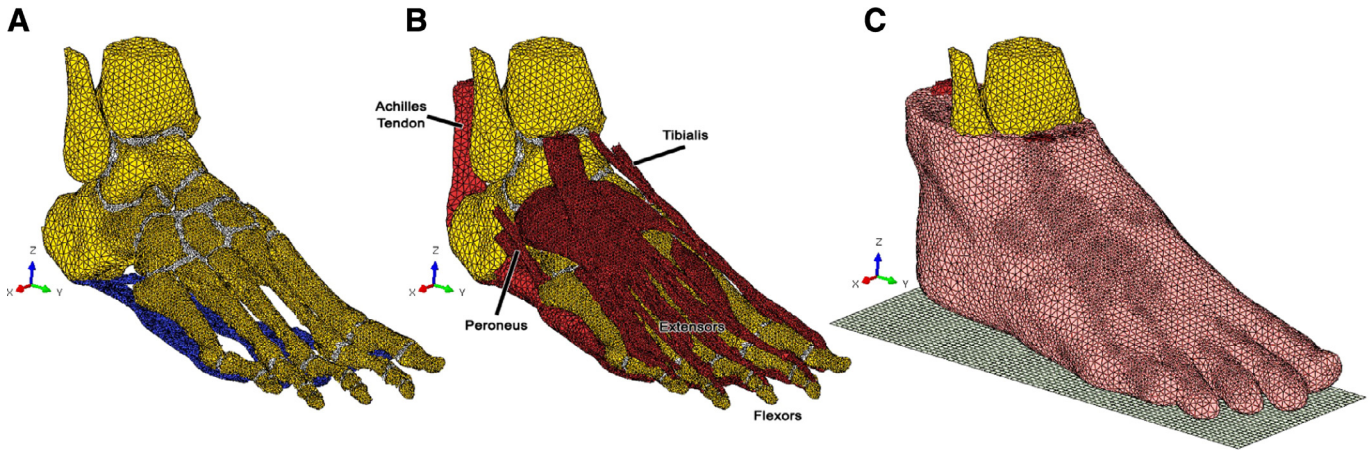

Fig. 1. Tissue layers of the finite element model. (A) Skeleton + fascia. (B) Skeleton + muscle/tendons. (C) Skeleton + soft tissue + ground.

Table 1
Mesh quality metrics based on Burkhart et al. [20] recommendations.

Mesh quality metric	Assessment criteria	Accurate elements	Inaccurate elements
Element Jacobians	>0.2	99.9%	0.1%
Aspect Ratio	<3	94.5%	5.5%
Min angles	>30°	80.2%	19.8%
Max angles	<120°	99.8%	0.2%

Table 2
Formulation approach for each tissue included in the model. Units for the shear parameters (μ and C_{ij}) are MPa and for the compressibility parameter (D_i) are $mm^2\,N^{-1}$.

Component	Constitutive model	Constants	Reference
Cortical bone	Linear elastic	$E = 17{,}000$ MPa, $\nu = 0.3$	[13]
Trabecular bone	Linear elastic	$E = 700$ MPa, $\nu = 0.3$	[13]
Rearfoot cartilages	Linear elastic	$E = 10$ MPa, $\nu = 0.4$	[43]
Forefoot cartilages	Linear elastic	$E = 1$ MPa, $\nu = 0.4$	[44]
Fascia	Linear elastic	$E = 350$ MPa, $\nu = 0.3$	[6]
Muscle	Linear elastic	$E = 450$ MPa, $\nu = 0.3$	[9]
Tendon	Ogden $n = 1$	$\mu = 33.1622$, $\alpha = 24.8987$, $D = 0.0001207$	–
Fat tissue	Hyperelastic $n = 2$	$C_{10} = 0.08556$, $C_{01} = -0.05841$, $C_{20} = 0.039$, $C_{11} = -0.02319$, $C_{02} = 0.00851$, $D_1 = 3.65273$, $D_2 = 0$	[45]

times, once for each different approach and the load-displacement curve obtained was compared with the experimental curve to evaluate the performance of each material model.

2.3. Foot finite element model validation

The biomechanical reliability of the model was evaluated by means of two different responses: vertical foot displacement and plantar pressure distribution.

The vertical displacement of the foot arch structure was evaluated with experimental measurements available in the literature. Cheung et al. [6] performed a pure vertical compression test in six cadaveric feet and the average of the six curves reported was used for comparison. Tao et al. [21] measured the vertical deformation of the foot in vivo under gradual increasing loads using a motion capture system. The model was loaded axially from 0 to 500 N in 100 N step increments (Table 3—Configuration 1) and the vertical displacement of the navicular bone was compared with both experimental measurements.

The plantar pressure distribution and location of the center of pressure (CoP) predicted by the model were matched with the measurements of the same subject who volunteered for scanning. The volunteer stood upright for 30 s on a pressure platform with 25 mm^2 resolution, model Footchecker (Loran Engineering S.R.L., Italy). Due to the slightly unbalanced standing of the volunteer during the record time, little variations were registered from one measure to another. Therefore, the most balanced distribution of three measurements was selected. The model was set up for standing position, i.e., half of the body weight and half of the tendon forces for midstance walking phase [22] (Table 3—Configuration 2).

2.4. Analyses

2.4.1. Tendon force sensitivity analysis

The idea behind the tendon force sensitivity analysis was to determine the impact of each tendon on the foot-ankle complex. Two sensitivity analyses were performed based on two different loading condition: standing position and midstance walking phase.

In the first sensitivity analysis, standing position, the tendon forces were set as in the previous case to calculate the plantar pressure distribution (Table 3—Configuration 2). Then, a sensitivity analysis of the five major stabilizer tendons was performed ranging their loads from 0 to 300 N individually in 100 N step increments and keeping the rest of the forces in standing configuration. In the second sensitivity analysis, midstance walking phase, the muscle forces were based on the estimation of Salathe and Arangio [22] and the axial load was fixed as 0.9 of the body weight [23]. Again, a sensitivity study of the stabilizer tendons from 0 to 300 N was performed (Table 3—Configuration 3).

Table 3
Load configurations applied to the model in total contact position for each analysis. Ellipses indicate the values that have been ranged in the sensitivity analysis keeping the rest of the tendon forces fixed. Force values are given in Newtons.

Loads	Conf. 1 Validation	Conf. 2 Standing position	Conf. 3 Midstance phase	Conf. 4 Early-midstance	Conf. 5 Late-midstance
Axial load	0 … 500	350	630	630	630
Achilles tendon	–	… 150 …	… 300 …	300	1300
Tibialis anterior	–	…–…	…–…	60	–
Tibialis posterior	–	… 30 …	… 60 …	60	60
Peroneus brevis	–	… 12 …	… 24 …	12	36
Peroneus longus	–	… 24 …	… 48 …	24	72
Extensor hallucis longus	–	15	30	60	30
Flexor hallucis longus	–	15	30	30	120
Extensor digitorum longus	–	7,5	15	30	15
Flexor digitorum longus	–	7,5	15	15	60

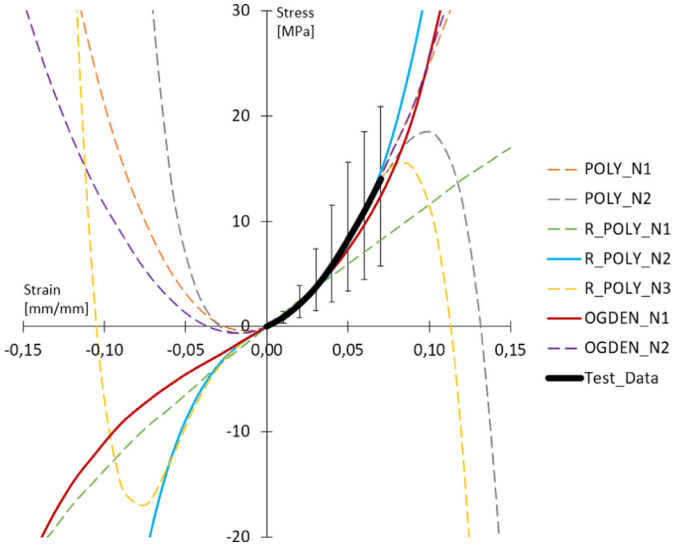

Fig. 2. Fitting curves of different material models for foot tendon tissue. Polynomial $n = 1$ and 2, polynomial reduced order 1, 2 and 3 and Ogden first and second order. The experimental curve is presented with mean and standard deviation [15].

2.4.2. Quasi-static analysis of walking midstance phase

The walking midstance phase comprehends about 50% of the stance phase of gait, from ~15% to ~65%, and within that period the muscular stimulus varies. At early-midstance, the musculature is disposed to impact absorption whereas at late-midstance the musculature is arranged to impulse. Hence, the beginning and the end of this phase were configured in order to study the effect of these alterations (Table 3—Configuration 4 and 5). The load conditions for these cases were estimated considering the midstance configuration and muscle activation patterns during walking [3].

3. Results

3.1. Tendon characterization

Out of the seven approaches chosen to fit the average foot tendon response, only first order Ogden formulation and polynomial reduced of second order fitted the experimental curve performing a real physiological behavior, i.e. compression stress with negative strains (Fig. 2). In the second step, where the uniaxial tendon tests were replicated, the Ogden material model showed better agreement with experimental data than the polynomial reduced of second order model. Therefore, the parameters of the first order Ogden material model were used to simulate foot tendon tissue.

Afterward, the model performance was evaluated comparing the force-displacement curve with foot tendon models used in the literature and the experimental curve of specific tendon tests. In Fig. 3 it is shown that only the hyperelastic material model adjusted in this study performs an actual non-linear behavior of tendon tissue in the toe region. The other hyperelastic approach, the two-parameter Mooney–Rivlin formulation, responded almost linearly. The material model fitted in this study reproduced better the actual non-linear behavior of foot tendons than previous approaches.

3.2. Foot finite element model validation

The model reproduced accurately the vertical displacement of the foot under compression predicting a non-linear response of the foot-ankle complex, i.e., becoming stiffer by increasing the axial load (Fig. 4). Regarding the plantar pressure distribution, a good match of peak value and location were found (Fig. 5). However, the CoP of the model was misaligned longitudinally and transversally with respect to the measured CoP. This deviation occurred because, in the simulation, the toes and the midfoot did not make ground contact, which displaced the predicted CoP medially and backward.

3.3. Analyses

3.3.1. Tendon force sensitivity analysis

The results of the sensitivity analysis of the five major stabilizer tendons were similar in both configurations, standing position and midstance phase. All tendons except the tibialis anterior plantarflexed the foot, producing a load transfer from rearfoot to forefoot such that the AT was the major contributor. The tibialis anterior dorsiflexed the foot. The tibialis and peroneus tendons also produced load transference in the frontal plane. The peroneus tendons everted the foot (the peroneus longus contributed most), increasing the plantar pressure under sesamoids, whereas the tibialis tendons relieved pressure under the first ray, inverting the foot (the tibialis anterior contributed most) (Fig. 6A). In the transverse plane, a similar response was observed. The peroneus tendons produced abduction while the tibialis tendons adducted the foot and the AT kept the foot equilibrated (Fig. 6B). The longitudinal arch was also influenced by muscular activity. The increase of AT force stressed the plantar fascia by increasing length and decreasing height of the arch. By contrary, the tibialis tendons reduced the stress in the plantar fascia by reducing the length and increasing the height of the arch. The tibialis posterior was more effective in this regard.

A coupled response of the eversion–inversion tendons was observed. When the force exerted in a peroneus or tibialis tendon was increased, the stress in the agonist tendon was reduced, while the stresses in the antagonists were increased. A similar response

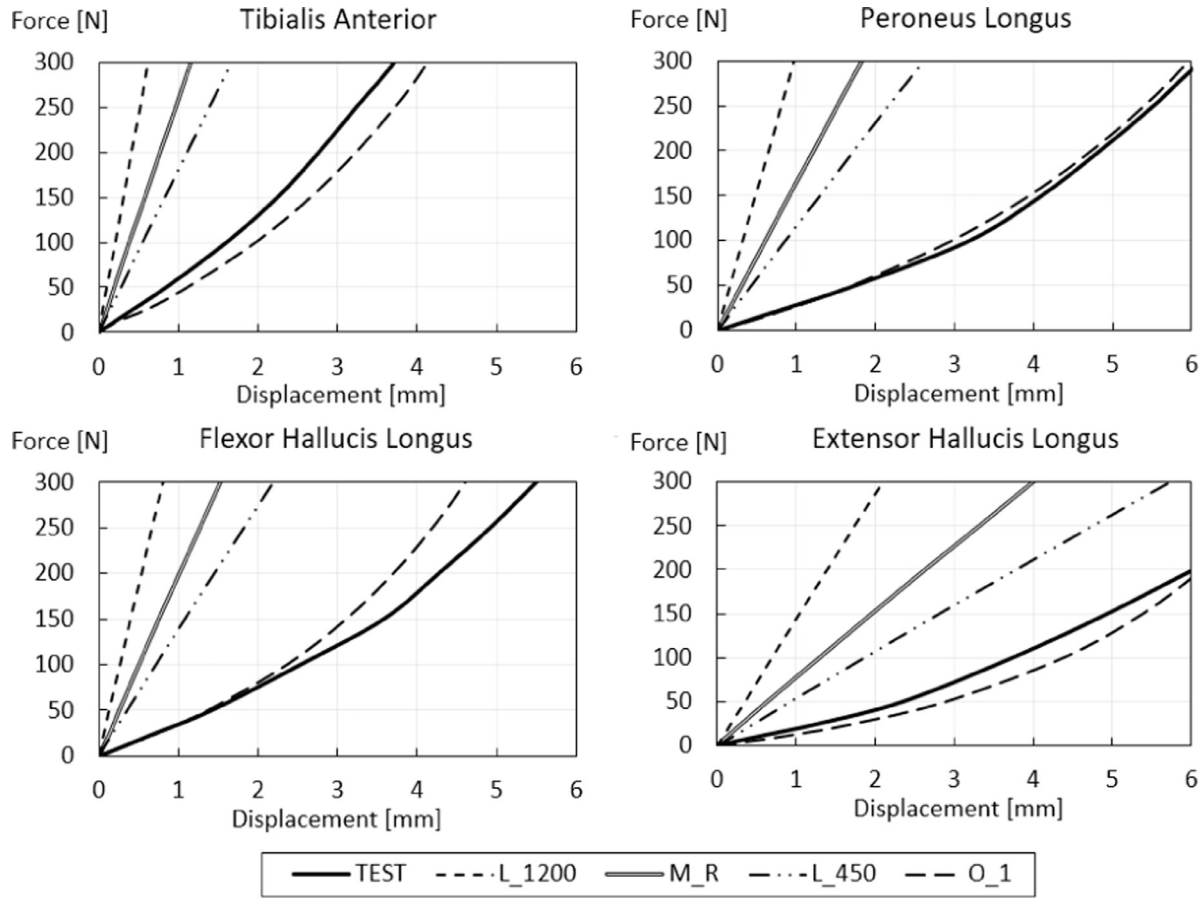

Fig. 3. Performance comparison of the different material models of foot tendon tissue used in the literature. The four experimental tendon curves were randomly selected from reference [15]. L_1200—Linear elastic isotropic Young's modulus 1200 MPa [11]. M_R—Hyperelastic Mooney–Rivlin [12]. L_450—Linear elastic isotropic Young's modulus 450 MPa [13]. O_1—Hyperelastic Ogden first order adjusted in this study.

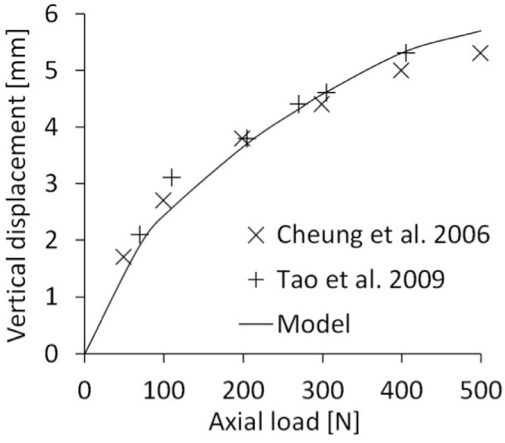

Fig. 4. Comparison of the vertical displacement measured by Cheung et al. [6] and Tao et al. [21] with the vertical displacement calculated by the model (Load configuration 1).

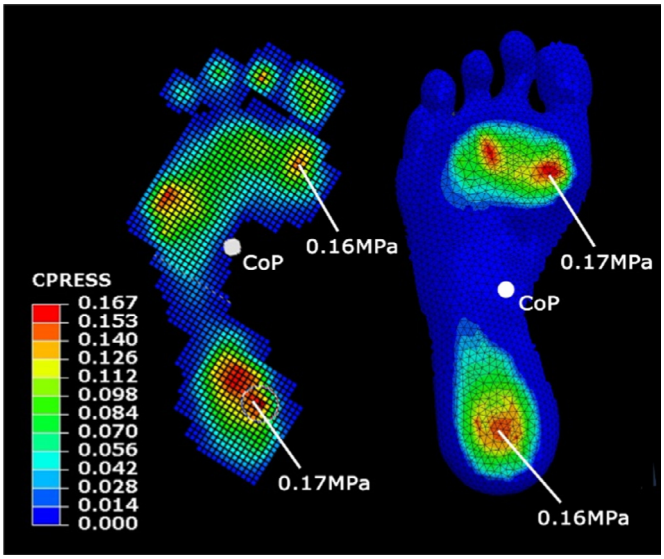

Fig. 5. Comparison of the plantar pressure measured (left) and the plantar pressure predicted (right) in upright standing position (Load configuration 2). CoP—Center of pressure.

was perceived between AT and tibialis anterior, such that pulling from one stressed the other one (Fig. 7).

3.3.2. Quasi-static analysis of walking midstance phase

From early to late-midstance positions mechanical solicitations were predicted. At the beginning of midstance, a peak plantar pressure of 0.26 MPa was estimated in the rearfoot. At the end, the contact area was reduced under the rearfoot and increased under the forefoot, reaching plantar pressure values of 0.6 MPa. The plantar fascia during midstance was stressed up to 3 MPa at 2 cm of the calcaneus insertion. In the talocrural joint cartilage, compression stress values of −5.6 MPa were predicted for late-midstance

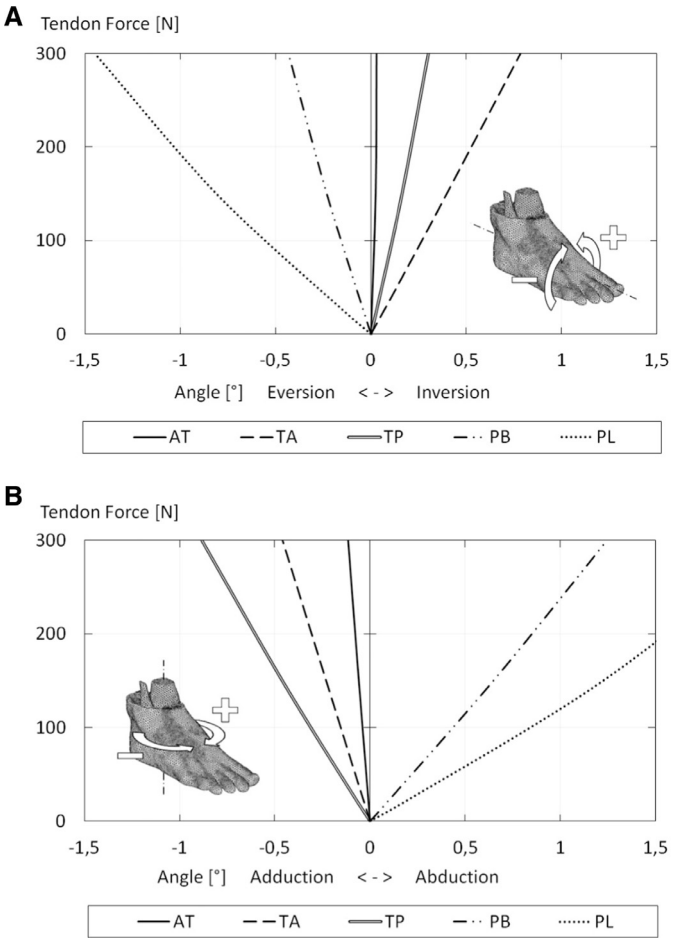

Fig. 6. Rotation angles of the foot as function of force exerted by tendons (Load configuration 3). (A) Eversion–inversion movement. (B) Adduction–abduction movement.
TA—Tibialis anterior, TP—Tibialis posterior, AT—Achilles tendon, PB—Peroneus brevis, PL—Peroneus longus.

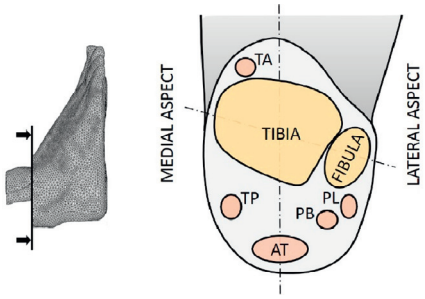

	Tibialis Anterior (TA)	Tibialis Posterior (TP)	Peroneus Longus (PL)	Peroneus Brevis (PB)	Achilles Tendon (AT)
Tibialis Anterior	▲	-	▼	▲	▲	▲
Tibialis Posterior	▲	▼	-	▼	▲	▲
Peroneus Longus	▲	▲	▲	-	▼	▼
Peroneus Brevis	▲	▼	▲	▲	-	▼
Achilles Tendon	▲	▲	▼	▼	▼	-

Fig. 7. Stabilizer tendon relationships. Above: Tendon location scheme on the cross-section of the ankle at talocrural-joint–high. Below: Tendon stress relationship observed in the sensitivity analysis. In each row, one tendon was pulled and the reaction of the other tendons is represented by increasing (▲) or decreasing stress (▼).

phase. With respect to the tendons, tibialis and peroneus tendons worked in values of 1–3 MPa during midstance cases and the AT reached 17.7 MPa at late-midstance analysis. In late-midstance position, higher mechanical response of the foot structure was required.

4. Discussion

In the present study, a complete foot FE model was developed including a detailed representation of the actual geometry and behavior of tendons. Trabecular and cortical bones were differentiated and each cartilage, fascia, tendon, and muscle that compounds the foot were included in the model, comprising 102 deformable volumes. Tendons were simulated with a non-linear first order Ogden material model adjusting the parameters with uniaxial tendon testing curves. Finally, the model was validated and the effect in the foot-ankle complex produced by the extrinsic tendons was assessed.

Input requirements of biomechanical models make necessary to quantify the force applied by each muscle-tendon-unit during a specific movement. Since there are no actual measurements of those forces in the literature, kinetic estimations have to be used. In the present study, the muscle forces calculated by Salathe and Arangio [22] were chosen as a reference to set the different loading conditions. These values are consistent with the range of force in which each tendon is expected to work; considering that tendons work regularly below half of its capacity the values proposed for midstance positions are below 15% of the load failure [15,24]. These values have been adopted previously for the computational simulation of flatfoot (Pes Planus) [25] and are similar to the values employed in other computational and cadaveric models estimated through different approaches [26,27].

The model predictions were validated in two different responses and showed good agreement with in-vivo and in-vitro measurements. This model is a step further in the development of foot FE models since it includes a more accurate simulation of the tendon tissue. This new feature opens new possibilities in the analysis of foot soft tissue function and pathology. In the literature there are abundant research studies related to the muscle-tendon activity during walking: capture motion measurements, electromyographic reports, musculoskeletal models estimations and dynamic cadaver performances, however, none of these methods measured tissue stress. Stress information is relevant because it is the mechanical parameter closely related to pain, tissue damage and mechanical stimuli of biochemical processes. The FE model presented in this study, based upon kinetic parameters, estimates tissue stress, an important contribution to the production of trustworthy information of clinical relevance.

The new model used in this study present some limitations that need to be addressed in future developments. A better simulation of bone-to-bone contact is necessary. There are two main approaches to deal with this interaction. One is the use of frictionless contact elements, which allow free movement between bones. This approach produces higher displacements between bony structures than in the experimental measures [6]. The other approach is to disregard contact properties of joints connecting one bone to another with low stiffness elements. The latter was used in this model and it has the limitation of making joint movements stiffer. Because of this option, ligaments were not simulated. Other features that should be improved to take full advantage of the model

are the soft tissue volume interactions. Within the foot-ankle complex, many muscle and tendon components overlap, limiting the displacement of one component respect to its surrounding. A slipping interaction between these components when a force is applied to a tendon would be desirable, although this feature represents a difficult computational challenge. In addition, remark that the results are susceptible to the force input data. Quantifying the forces exerted by each muscle during lower limb movements is a challenging task. Actual measurements on this matter are difficult to find in the literature because measuring muscle forces in vivo is generally not feasible. Therefore, the use of optimization algorithms based on physiological parameters is a recurrent way to predict tendon pulling forces. Due to the nature of those estimations, proposed values are within a large range and variability increases by inter-subject differences, age, and gender dependency. Therefore, advances in that direction will also improve the fidelity of the model.

Tissues are composite materials with sophisticated non-linear properties. Due to the limitation of the computational capacity a balance between the intricate geometry and the material properties used is necessary [2]. Foot FE models with detailed geometry usually include linear material properties to compensate the complexity of the mesh regarding the computational cost [28]. Recent models present improvements to reduce the gap between the simulation and the reality, as in the case of the present study for tendons and others for fascia [29] or for cartilages [30]. All these efforts together with the advances in computational capacity will give us the capacity to model the human foot with all its complexities.

The present model calculated the inversion–eversion movements of the foot relative to the tibia as a function of tendon forces. The peroneus tendons increased plantar pressure under the medial aspect and the tibialis tendons increased plantar pressure under the lateral aspect. At the ankle articular cartilage, the reverse was true, peroneus stressed lateral side while tibialis stressed medial side. This pattern was noted by Potthast et al. [31] measuring the effect of the muscle forces in the intraarticular pressure distribution of the talocrural joint. They concluded that the coupled activation of synergist tendons would intensify those changes. The FE model predicted cartilage peak stress values of this joint higher than the measurements reported for similar axial load ratios [32,33]. This overestimation could be expected since the linear material model applied to simulate the cartilage behavior was a gross approximation for this complex tissue. A refined formulation for these components will provide better results.

In the cadaveric simulation performed by Sharkey et al. [34], a mirror effect was described with respect to the sagittal plane. Load settings that produced high medial strains tended to produce low strains on the lateral side. This effect was also noted in our simulations, but besides a combined work of the tendons to keep the ankle movement stable. This coupled activation pattern of tendons is understandable given the precise control motion requirements to reach the responsiveness of the foot-ankle complex.

The arch-supporting function of the tibialis posterior is a common discussion in the literature [35–37]. However, the capacity of tibialis anterior of avoiding excessive navicular drop has not been well studied yet. The model predicted similar functions for the tibialis anterior than for the tibialis posterior although in a lesser degree. Future research in this line could open new possibilities for the treatment or preservation of pes planus.

Regarding the midstance analysis, it was observed that the foot is subjected to higher mechanical stresses during late-midstance previous to the heel rise. Stress in the plantar fascia was predicted in the proximal portion where plantar fasciitis is more likely to occur. The AT stress value predicted at the late-midstance position was similar to the 19 MPa maximal tension stress during walking measured by Finni et al. [38]. The stress levels estimated for the rest of the tendons constituted around 10% of their ultimate tensile stresses [15]. Considering that biological tissues, in their physiological performance, work below half the failure stress, these levels of solicitation are reasonable for a relatively low mechanical demand activity such as walking.

From a clinical perspective, the model can be applied to many pathological or dysfunctional conditions, such as altered muscle activation patterns. The present model-based findings also provide clinically relevant information on the role of the ankle muscles on pronation-supination. Health professionals are frequently interested in walking mechanisms that may decrease excessive pronation during early stance and may produce supination during late stance, in order to treat or prevent pathological conditions such as plantar fasciitis and medial tibial stress syndrome [39,40]. According to the present findings, at early-midstance, the ankle muscles produce a total torque of inversion and adduction, i.e., supination, while it is known that the foot is pronating at this instant [41]. Thus, these muscles decelerate pronation at early midstance and this function should be clinically optimized to avoid excessive pronation. The present results also showed that, at late-midstance, the ankle muscles, mostly demanded to generate plantar flexion and gait propulsion, produce a total torque of eversion and abduction, i.e., pronation. At this instant, the foot is actually supinating [41], what would be decelerated by the ankle muscles. Therefore, to optimize supination at late-midstance, the role of tissues other than ankle muscles should be also regarded. Lower-limb external rotation produced at the hip and its role in increasing supination [42], through the mechanical coupling between shank external rotation and foot supination [41], should be then clinically considered.

5. Conclusions

In this study, a three-dimensional FE model of the human foot, taking into account the real geometry and non-linear behavior of tendons, was developed and validated. The new features of the model focus in tendon stress estimation were used to shed light on the role of the five major stabilizer tendons and their impact in the foot-ankle complex. The model fed with kinetic data provides the mechanical response of each of the foot components. The model output is strongly related to the load tendon setting. Therefore, advances in muscle control force quantification during different lower limb movements will significantly help for more reliable predictions of the model.

The work was framed in the area of orthopedic biomechanics and was intended to advance towards a refined simulation of the internal soft tissues of the foot to predict therapy outcomes. Advances in biomechanical modeling will provide useful tools for clinical assessment, reducing cost and health hazards.

Ethics approval

Ethical approval for this study was granted by Bioethical Research Committee of the Hospital Clinico San Carlos at Complutense University (reference number 12/210-E). The volunteer gave written informed consent for participating in the computer tomographies and magnetic resonance imaging scanning and plantar pressure measurements.

Conflicts of interests

The authors have no conflicts of interest to declare.

Acknowledgments

The authors would like to thank Dr. Ricardo Becerro de Bengoa Vallejo and Dr. Marta Losa Iglesias for providing the computer tomographies, magnetic resonance images and plantar pressure measurements of the volunteer. Enrique Morales Orcajo was partially funded by the Brazilian Government—Coordenação de Aperfeiçoamento de Pessoal de Nivel Superior (CAPES). The study has been support by the Ministry of Economy and competitiveness of the Government of Spain through the project DPI2013-44987-R.

Supplementary materials

Supplementary material associated with this article can be found, in the online version, at doi:10.1016/j.medengphy.2017.07.010.

References

[1] Fontanella CG, Favaretto E, Carniel EL, Natali AN. Constitutive formulation and numerical analysis of the biomechanical behaviour of forefoot plantar soft tissue. J Eng Med 2014;228:942–51. doi:10.1177/0954411914551852.
[2] Morales-Orcajo E, Bayod J, Barbosa de Las Casas E. Computational foot modeling: scope and applications. Arch Comput Methods Eng 2016;23:389–416. doi:10.1007/s11831-015-9146-z.
[3] Sharkey NA, Hamel AJ. A dynamic cadaver model of the stance phase of gait: performance characteristics and kinetic validation. Clin Biomech 1998;13:420–33.
[4] Neptune RR, Kautz SA, Zajac FE. Contributions of the individual ankle plantar flexors to support, forward progression and swing initiation during walking. J Biomech 2001;34:1387–98. doi:10.1016/S0021-9290(01)00105-1.
[5] Murley GS, Menz HB, Landorf KB. Electromyographic patterns of tibialis posterior and related muscles when walking at different speeds. Gait Posture 2014;39:1080–5. doi:10.1016/j.gaitpost.2014.01.018.
[6] Cheung JT-M, Zhang M, An K-N. Effect of Achilles tendon loading on plantar fascia tension in the standing foot. Clin Biomech 2006;21:194–203. doi:10.1016/j.clinbiomech.2005.09.016.
[7] Chen Y-N, Chang C-W, Li C-T, Chang C-H, Lin C-F. Finite element analysis of plantar fascia during walking: a quasi-static simulation. Foot Ankle Int 2014;36:90–7. doi:10.1177/1071100714549189.
[8] Isvilanonda V, Dengler E, Iaquinto JM, Sangeorzan BJ, Ledoux WR. Finite element analysis of the foot: model validation and comparison between two common treatments of the clawed hallux deformity. Clin Biomech 2012;27:837–44. doi:10.1016/j.clinbiomech.2012.05.005.
[9] Morales-Orcajo E, Bayod J, Becerro-de-Bengoa-Vallejo R, Losa-Iglesias M, Doblare M. Influence of first proximal phalanx geometry on hallux valgus deformity: a finite element analysis. Med Biol Eng Comput 2015;53:645–53. doi:10.1007/s11517-015-1260-4.
[10] Chen W-M, Park J, Park S-B, Shim VP-W, Lee T. Role of gastrocnemius-soleus muscle in forefoot force transmission at heel rise—a 3D finite element analysis. J Biomech 2012;45:1783–9. doi:10.1016/j.jbiomech.2012.04.024.
[11] Wu L. Nonlinear finite element analysis for musculoskeletal biomechanics of medial and lateral plantar longitudinal arch of Virtual Chinese Human after plantar ligamentous structure failures. Clin Biomech 2007;22:221–9. doi:10.1016/j.clinbiomech.2006.09.009.
[12] Gu YD, Li JS, Lake MJ, Ren XJ, Zeng YJ. The mechanical response of Achilles tendon during different kinds of sports. Commun Numer Methods Eng 2008;24:2077–85. doi:10.1002/cnm.
[13] García-Aznar JM, Bayod J, Rosas A, Larrainzar R, García-Bógalo R, Doblaré M, et al. Load transfer mechanism for different metatarsal geometries: a finite element study. J Biomech Eng 2009;131:21011. doi:10.1115/1.3005174.
[14] Wang JH-C. Mechanobiology of tendon. J Biomech 2006;39:1563–82. doi:10.1016/j.jbiomech.2005.05.011.
[15] Morales-Orcajo E, Becerro De Bengoa Vallejo R, Losa Iglesias M, Bayod J. Structural and material properties of human foot tendons. Clin Biomech 2016;37:1–6. doi:10.1016/j.clinbiomech.2016.05.014.
[16] Shin J, Yue N, Untaroiu CD. A finite element model of the foot and ankle for automotive impact applications. Ann Biomed Eng 2012;40:2519–31. doi:10.1007/s10439-012-0607-3.
[17] Fernandes R, Aguiar R, Trudell D, Resnick D. Tendons in the plantar aspect of the foot: MR imaging and anatomic correlation in cadavers. Skeletal Radiol 2007;36:115–22. doi:10.1007/s00256-006-0203-4.
[18] Sarrafian SK. Anatomy of the foot and ankle. Descriptive, topographic, functional. Ed. 2. 1993.
[19] Michaud TC. Human locomotion: the conservative management of gait-related disorders; 2011.
[20] Burkhart TA, Andrews DM, Dunning CE. Finite element modeling mesh quality, energy balance and validation methods: a review with recommendations associated with the modeling of bone tissue. J Biomech 2013;46:1477–88. doi:10.1016/j.jbiomech.2013.03.022.
[21] Tao K, Wang D, Wang C, Wang X, Liu A, Nester CJ, et al. An in vivo experimental validation of a computational model of human foot. J Bionic Eng 2009;6:387–97. doi:10.1016/s1672-6529(08)60138-9.
[22] Salathe EP, Arangio GA. A biomechanical model of the foot: the role of muscles, tendons, and ligaments. J Biomech Eng 2002;124:281. doi:10.1115/1.1468865.
[23] Barela AMF, De Freitas PB, Celestino ML, Camargo MR, Barela JA. Ground reaction forces during level ground walking with body weight unloading. Braz J Phys Ther 2014;18:572–9.
[24] Wren TA, Yerby SA, Beaupré GS, Carter DR. Mechanical properties of the human Achilles tendon. Clin Biomech 2001;16:245–51.
[25] Wang Z, Imai K, Kido M, Ikoma K, Hirai S. A finite element model of flatfoot (Pes Planus) for improving surgical plan. Conf proc annu int conf IEEE eng med biol soc IEEE eng med biol soc annu conf 2014; 2014. p. 844–847. doi:10.1109/EMBC.2014.6943723.
[26] Imhauser CW, Siegler S, Abidi NA, Frankel DZ. The effect of posterior tibialis tendon dysfunction on the plantar pressure characteristics and the kinematics of the arch and the hindfoot. Clin Biomech 2004;19:161–9. doi:10.1016/j.clinbiomech.2003.10.007.
[27] Liu X, Zhang M. Redistribution of knee stress using laterally wedged insole intervention: finite element analysis of knee-ankle-foot complex. Clin Biomech 2013;28:61–7. doi:10.1016/j.clinbiomech.2012.10.004.
[28] Wong DW-C, Niu W, Wang Y, Zhang M. Finite element analysis of foot and ankle impact injury: risk evaluation of calcaneus and talus fracture. PLoS One 2016;11:e0154435. doi:10.1371/journal.pone.0154435.
[29] Lin S-C, Chen CP-C, Tang SF-T, Chen C-W, Wang J-J, Hsu C-C, et al. Stress distribution within the plantar aponeurosis during walking—a dynamic finite element analysis. J Mech Med Biol 2014;14:1450053. doi:10.1142/S0219519414500535.
[30] Marchelli GLS, Ledoux WR, Isvilanonda V, Ganter MA, Storti DW. Joint-specific distance thresholds for patient-specific approximations of articular cartilage modeling in the first ray of the foot. Med Biol Eng Comput 2014;52:773–9. doi:10.1007/s11517-014-1179-1.
[31] Potthast W, Lersch C, Segesser B, Koebke J, Brüggemann GP. Intraarticular pressure distribution in the talocrural joint is related to lower leg muscle forces. Clin Biomech 2008;23:632–9. doi:10.1016/j.clinbiomech.2007.11.005.
[32] Calhoun JH, Li F, Ledbetter BR, Viegas SF. A comprehensive study of pressure distribution in the ankle joint with inversion and eversion. Foot Ankle Int 1994;15:125–33. doi:10.1177/107110079401500307.
[33] Natsakis T, Burg J, Dereymaeker G, Vander Sloten J, Jonkers I. Extrinsic muscle forces affect ankle loading before and after total ankle arthroplasty. Clin Orthop Relat Res 2015. doi:10.1007/s11999-015-4346-2.
[34] Sharkey N, Ferris L, Smith T, Matthews D. Strain and loading of the second metatarsal during heel-lift. J Bone Joint Surg 1995;77A:1050–7.
[35] Thordarson DB, Schmotzer H, Chon J, Peters J. Dynamic support of the human longitudinal arch—a biomechanical evaluation. Clin Orthop Relat Res 1995;316:165–72.
[36] Kitaoka H, Luo Z, An K. Effect of the posterior tibial tendon on the arch of the foot during simulated weightbearing: biomechanical analysis. Foot Ankle Int 1997;18:43–6.
[37] Watanabe K, Kitaoka HB, Fujii T, Crevoisier X, Berglund LJ, Zhao KD, et al. Posterior tibial tendon dysfunction and flatfoot: analysis with simulated walking. Gait Posture 2013;37:264–8. doi:10.1016/j.gaitpost.2012.07.015.
[38] Finni T, Komi P, Lukkariniemi J. Achilles tendon loading during walking: application of a novel optic fiber technique. Eur J Appl Physiol 1998;77:289–91.
[39] Chang R, Rodrigues PA, Van Emmerik REA, Hamill J. Multi-segment foot kinematics and ground reaction forces during gait of individuals with plantar fasciitis. J Biomech 2014;47:2571–7. doi:10.1016/j.jbiomech.2014.06.003.
[40] Neal BS, Griffiths IB, Dowling GJ, Murley GS, Munteanu SE, Franettovich Smith MM, et al. Foot posture as a risk factor for lower limb overuse injury: a systematic review and meta-analysis. J Foot Ankle Res 2014;7:1–13. doi:10.1186/s13047-014-0055-4.
[41] Souza TR, Pinto RZ, Trede RG, Kirkwood RN, Fonseca ST. Temporal couplings between rearfoot-shank complex and hip joint during walking. Clin Biomech 2010;25:745–8. doi:10.1016/j.clinbiomech.2010.04.012.
[42] Souza TR, Mancini MC, Araújo VL, Carvalhais VOC, Ocarino JM, Silva PL, et al. Clinical measures of hip and foot-ankle mechanics as predictors of rearfoot motion and posture. Man Ther 2014;19:379–85. doi:10.1016/j.math.2013.10.003.
[43] Gefen A. Stress analysis of the standing foot following surgical plantar fascia release. J Biomech 2002;35:629–37. doi:10.1016/s0021-9290(01)00242-1.
[44] Athanasiou KA, Liu GT, Lavery LA, Lanctot DR, Schenck RC. Biomechanical topography of human articular cartilage in the first metatarsophalangeal joint. Clin Orthop Relat Res 1998;348:269–81.
[45] Chen W-M, Lee T, Lee PV-S, Lee JW, Lee S-J. Effects of internal stress concentrations in plantar soft-tissue—a preliminary three-dimensional finite element analysis. Med Eng Phys 2010;32:324–31. doi:10.1016/j.medengphy.2010.01.001.